

The mitigating effect of selenium against lead-induced neurotoxicity in the cerebellar cortex of adult male albino rats

Abdelmonem A. Hegazy^{1,2}, Dalia I. El-wafaey¹, Fatma Akmal¹, Ayat M. Domouky¹

¹ Human Anatomy and Embryology Department, Faculty of Medicine, Zagazig University, Zagazig City 44519, Egypt

² Human biology, Basic Medical Science Department, Faculty of Dentistry, Zarqa University, Zarqa City 13110, Jordan

SUMMARY

Lead (Pb)-induced neurotoxicity is a major public health problem. The nervous system is the primary target of Pb toxicity. Since selenium (Se) has anti-inflammatory and antioxidant effects that have been shown to provide some protection against heavy metal toxicity, the present study aimed to demonstrate the potential protective role of Se against the effects of Pb on the cerebellar structure of rats using histopathological, immunohistochemical, biochemical and molecular measures. Experimental rats were divided into 3 groups, each divided into 2 subgroups: control group (Se-free and Se-supplemented subgroups), Pb group (low and high dose Pb subgroups), and Pb/Se group (low and high dose Pb subgroups with Se). After 4 weeks of administration, cerebellar samples were collected for investigation. Pb-induced cerebellar damage was manifested by significant increases in the glial fibrillary acidic protein (GFAP), brain oxidative marker (malondialdehyde) and apoptosis (DNA fragmentation), particularly at high dose. Pb also caused alteration of normal cerebellar structure and cellular degeneration with a significant reduction in the total number of Purkinje cells and the thickness of mo-

lecular and granular layers. All these alterations were greatly mitigated by co-administration of Se especially in the low dose Pb/Se subgroup. Se has been suggested to reduce Pb-induced neurotoxicity in the cerebellum. Further experimental studies are recommended before applying the results in clinical trials.

Key words: Lead toxicity – Cerebellum – Oxidative stress – Antioxidant – DNA degradation – Apoptotic

INTRODUCTION

Heavy metals pose serious challenges to environmental soil quality, and affect human health across the food chain (Xu et al., 2023). Lead (Pb) is one of the most common neurotoxic metals in the environment (Li et al., 2023). High concentrations of Pb in drinkable water continue to cause Pb poisoning crises. Drinking water should not contain more than 0.01 mg/L of Pb (Wang et al., 2023). However, Pb concentrations in the groundwater samples studied ranged from 90 to 410 grams per liter on average (Salman et al., 2019). Pb enters the environment through many sources, including gasoline, dust, jet fuel, drinking water through leaded pipes, food products, cosmetics, and dish-

Corresponding author:

Abdelmonem Awad Hegazy. Professor of Human Anatomy and Embryology Department, Faculty of Medicine, Zagazig University, Zagazig City 44519, Egypt. / Human biology, Basic Medical Science, Department, Faculty of Dentistry, Zarqa University, Zarqa City 13110, Jordan. Phone: +201110504321. E-mails: ahgazy@zu.edu.eg / dr.abdelmonemhegazy@yahoo.com - ORCID: 0000-0002-5993-6618.

Submitted: August 24, 2025. Accepted: November 6, 2025

<https://doi.org/10.52083/MFIW1839>

es containing Pb enamel (Ranjbar et al. 2023). Ingesting high levels of Pb can lead to health risks, including neurotoxicity, liver and kidney damage, and bowel disorders (Ademuyiw et al., 2007). Compared to other organs, the nervous system is the most sensitive and the first target of Pb poisoning (Singh et al., 2017). Due to its ability to substitute calcium ions, Pb can cross the blood-brain barrier (BBB) (Ghaderi et al., 2023). Pb also has the ability to induce apoptosis (Galal et al., 2019). Furthermore, Pb toxicity can alter antioxidant homeostasis, leading to increased free radical generation and lipid peroxidation, resulting in oxidative stress. Because of the extremely high rate of oxygen consumption in the brain, the high levels of unsaturated fatty acids as substrates for lipid peroxidation, and the non-regenerative nature of neurons, the brain is very vulnerable to oxidative stress (Nehru and Kanwar, 2004).

Selenium (Se) is a trace mineral, found ubiquitous in the environment and of fundamental importance to human health. Se plays a unique and important role among trace elements as the only element that is genetically encoded in proteins and a component of the 21st amino acid, selenocysteine. It is found as selenocysteine in the active sites of Se-dependent enzymes such as thioredoxin reductases, glutathione peroxidases, and iodothyronine deiodinases. Proteins that contain at least one selenocysteine residue in their structure are called selenoproteins, which perform many important physiological roles, the main function of which is to maintain the redox balance in cells (Genchi et al., 2023). The main source of Se for humans is the diet, such as grains, meat, and seafood (Ullah et al., 2018). In fresh water, Se occupies a concentration range of 0.2 to 10 grams per liter, and in sea water, about 0.09 grams per liter. Selenomethionine, selenocysteine, and selenocysteine are organic compounds that contain Se. Therefore, the organic form of Se has previously been recommended as the primary form of Se supplements for its antioxidant and anti-inflammatory activity (Ali et al., 2020, Khalil et al., 2023). Se has been shown to reduce the formation of reactive oxygen species (ROS), protect cells from glutamate toxicity, oxidative stress, and inflammatory cytokines, thus preventing cell death in-

duced by these conditions (Ma et al., 2017). It also protects against ischemic damage by reducing DNA oxidation, restoring mitochondrial function, or preventing autophagy (Zhuo et al., 2023). Furthermore, Se has been found in experiments to protect against methylmercury toxicity (Ralston and Raymond, 2010). The potential protective effect of Se against Pb-induced cortical damage was also reported in a previous study (Hegazy et al., 2023).

The cerebellum and cerebrum exhibit different responses to pathogens, particularly about BBB permeability and immune cell infiltration, with the cerebellum showing more extensive and prolonged BBB permeability compared to the cerebral cortex (Phares et al., 2006). Additionally, the cerebellum neurons represent more than half of the neurons in the entire nervous system (Carey, 2024). This network of neurons communicates with many other brain structures, and influences not only motor functions including posture, coordination, and motor learning but also non-motor functions such as sensory, autonomic, cognitive, and emotional processes (Prati et al., 2024). Furthermore, sex-dependent neurodevelopmental disorders have been reported in mice due to maternal Pb exposure, affecting male offspring more severely (Choi et al., 2022). Therefore, the aim of the present experiment was to evaluate the effect of low- and high-dose Pb on the cerebellar structure of adult male rats, and to elucidate the potential protective role of Se in ameliorating this damage using histopathological, immunohistochemical, biochemical and molecular methods.

MATERIALS AND METHODS

Chemicals

Pb acetate 99% was purchased from Piochem Company. Se Sodium selenite white to off-white powder soluble in water, more than 98% of purity was purchased from Sigma Aldrich, USA. Distilled water was gotten from Kemecta Company.

Animals

Sixty mature male albino rats, each weighing 150–250 grams each, were used in the investigation. They were obtained from the Faculty of

Medicine's Animal House. The rats had unfettered access to regular food and water while being kept in hygienic, controlled environments. The temperature in their hygienic enclosures was maintained at 22°C. The animals were allowed to acclimatize to the laboratory setting for two weeks before the experiment. The Institutional Animal Care and Use Committee (IACUC) of the University accepted the experimental protocol (Approval No. ZU-IACUC/3/F/93/2020), and all procedures adhered to the National Institutes of Health's (NIH) animal care guidelines.

Experiment protocol

The animals were randomly divided into 3 groups, 20 rats in each group (control group, Pb group, and Pb/Se group). Each group was then divided into two subgroups (10 rats in each subgroup). Control group included Se-free subgroup, received no treatment and Se subgroup, received 0.25 mg/kg/day of Se by oral gavage (Adedara et al., 2020). Pb group included low doses Pb subgroup (L-Pb), received 20ml/kg/day of Pb acetate dissolved in 1ml distilled water by oral gavage (Baty et al., 2020) and high doses Pb subgroup (H-Pb), received 50ml/kg/day of Pb acetate dissolved in 1ml distilled water by oral gavage (Hamdan et al., 2020). Pb/Se group included low doses Pb and Se subgroup (L-Pb/Se), received 20 mg/kg/day of Pb acetate along with 0.25 mg/kg/day of Se by oral gavage, and high doses Pb and Se subgroup (H-Pb/Se), received 50 mg/kg/day of Pb acetate along with 0.25 mg/kg/day of Se by oral gavage. The chemicals were given to the animals daily throughout the four-week experiment.

Sample preparation

All animals were anesthetized by intraperitoneal injection of 30 mg/kg thiopental (IACUC 2014), twenty-four hours after the last dose of the treatment substance, the cerebellum was carefully excised and divided into 3 equal parts.

The first cerebellar sections (middle part, including the vermis) were wrapped in aluminum foil and frozen at -80°C until needed for biochemical examination, while the second cerebellar segments (extracted from left cerebellar hemisphere)

were prepared for histopathological examinations using light microscopy (LM). The third cerebellar segments (extracted from right cerebellar hemisphere) were prepared for electron microscopy (EM) examinations.

Comet assay for DNA fragmentation

The degree of DNA migration and the percentage of migrated DNA can be used to quantitatively and qualitatively evaluate DNA damage in treated cells. Kinetic Imaging Ltd. (Liverpool, UK) created the Comet 5 image processing software, which was used in conjunction with a CCD camera for this analysis (Tice et al., 2000).

Homogenate tissue analysis

The tissues were spun for 30 minutes at 5000 rpm after being homogenized five times their tissue weight in ice-cold phosphate buffers (50 mM, pH 7.4). After that, the supernatants were kept in a deep freezer until they were needed for the subsequent tests. Lipid peroxidation assay: Cerebellar homogenate samples will be mixed with TBA (0.2 percent) in H₂SO₄ (0.05 M) and heated for 30 minutes in a boiling water bath. Thiobarbituric acid-reactive molecules were extracted using N-butanol, and absorbance at 532 nm was determined. Malonaldehyde (MDA) served as reference, and the results were expressed in nmol/mg protein (Nili-Ahmadabadi et al., 2018). Total antioxidant capacity (TAC) assay: samples were evaluated based on their capability to convert Fe³⁺ to Fe²⁺. With a peak absorption of 593 nm, the Fe²⁺ and TPTZ complex generated a blue hue. Nanomoles per milligram of protein was the unit of measurement used for the results (Nili-Ahmadabadi et al., 2018).

LM and morphometric examination

The cerebellar specimens were fixed in 10% paraformaldehyde in phosphate buffer (PH=7.4) for 48 hours. In ascending grades of alcohol (50%, 70%, 90% and 95%), the specimens were then dehydrated for one hour. Subsequently, in absolute alcohol (100%), two changes of 1 h each were made. After clearing in xylene, specimens were embedded in soft paraffin wax at 55 °C for 2 hours and in hard paraffin at 60 °C for another 2 hours.

Sections of 5 μm thick were prepared for staining with Hematoxylin and Eosin (H&E) (Bancroft and Gamble 2008; Hegazy and Hegazy 2015). Cerebellar sections were examined using a LM and then photographed. Histological images were analyzed using ImageJ software (ImageJ/Fiji 1.46r, <https://imagej.nih.gov/ij/index.html>) for: 1) Thickness of molecular and granular layers at 100 \times magnification. 2) Total number of Purkinje cells per field; at 400 \times magnification.

EM examination

Following a few hours of immersion in 3% glutaraldehyde in 0.1M phosphate buffer, cerebellar slices from each group were fixed for an hour in 1% osmium tetroxide. An ultrathin microtome was used to cut 50 nm-thick sections from specific regions, which were then contrasted with Pb citrate and uranyl acetate (Bancroft and Gamble 2008). An AMT CCD camera (software version AMTV600) was used to take pictures, and sections were inspected under JEM-2100.

Immunohistochemical analysis

Immunohistochemistry was performed using the streptavidin–biotin immunoperoxidase technique. Sections 3–5 μm thick were created by mounting formalin-fixed, paraffin-embedded blocks on positively charged glass slides, deparaffinizing them in xylene, and then rehydrating them in graded alcohol. Heat-induced antigen retrieval was carried out for 20 minutes in citrate buffer at PH 6. Sections were washed in phosphate buffered saline (PBS) after being treated with 3% hydrogen peroxide for 10 minutes to prevent endogenous peroxidase activity. After that, the slides were treated for the entire night with primary antibodies. Sigma Laboratories provided the polyclonal rabbit anti-glial fibrillary acidic protein (anti-GFAP).

Novacastra Laboratories Ltd.'s avidin biotin peroxidase technology was utilized in the universal kit. Diaminobenzidine chromogen was used for product visualization and secondary antibody incubation. Slides were counterstained with Mayer's hematoxylin and cleaned with PBS and distilled water. As negative controls, PBS was utilized in place of the main antibody (Olga et al 2002;

Bancroft and Gamble, 2008). In order to facilitate blind examination and evaluation under LM, ten fields from three distinct non-overlapping horizontal sections of each rat were coded and photographed.

Statistical analysis

SPSS version 18.0 was used to statistically analyze all of the data. The data distribution's normality was evaluated using the Shapiro-Wilk test. One-way ANOVA was used to compare group means for normally distributed data, and the Tukey HSD post-hoc test was used for multiple comparisons. The findings were presented in the form of mean \pm SD. The Mann-Whitney test was utilized for post-hoc analysis, and the Kruskal-Wallis H test was utilized to compare group medians for data that did not follow a normal distribution. Median values with ranges were used to display these findings. P-values below 0.05 were deemed statistically significant.

RESULTS

DNA fragmentation results

The cerebellar DNA fragmentation (tailed, tail length, tail DNA, and tail moment) was significantly increased in rats treated with Pb only (L-Pb) and H-Pb subgroups, and rats treated with Pb and Se (L-Pb/Se) and H-Pb/Se subgroups comparing to control group. The cerebellar DNA fragmentation was significantly reduced in the L-Pb/Se subgroup when Pb and Se were combined, compared to the L-Pb subgroup. Additionally, compared to the H-Pb subgroup, the H-Pb/Se subgroup's combination of Pb and Se demonstrated a significant decrease in cerebellar DNA fragmentation (tailed, tail length, tail DNA, and tail moment) (Table 1).

Lipid peroxidation results

In terms of malondialdehyde (MDA) biochemical examination, the cerebellar MDA levels of the L-Pb, H-Pb, L-Pb/Se, and H-Pb/Se subgroups were significantly higher than those of the Se-free subgroup. Cerebellum MDA was significantly lower in the L-Pb/Se and H-Pb/Se subgroups than in the L-Pb and H-Pb subgroups, respectively (Table 1).

Table 1. DNA fragmentation and biochemical analysis results in different study groups

	Control group		Pb group		Pb/Se group		P value
	Se-free subgroup (n=10)	Se subgroup (n=10)	L-Pb subgroup (n=10)	H(Pb) subgroup (n=10)	L-Pb/Se subgroup (n=10)	H-Pb/Se subgroup (n=10)	
DNA fragmentation							
Tailed (%)	3.4±1.14	3.8±0.84	9.4±1.14 ^b	16.2±2.17 ^b	6.2±0.84 ^{ac}	10.4±1.14 ^{bf}	<0.001
Untailed (%)	96.6±1.14	96.2±0.84	90.6±1.14 ^b	83.8±2.17 ^b	93.8±0.84 ^{ac}	89.6±1.14 ^{bf}	<0.001
Tail length (um)	1±0.04	1.02±0.09	3.08±0.05 ^b	4.27±0.1 ^b	1.68±0.55 ^{ad}	3.06±.06 ^{bf}	<0.001
Tail DNA (%)	1.11±0.03	1.16±0.06	2.68±0.06 ^b	3.73±0.33 ^b	1.72±0.51 ^{ad}	2.92±0.12 ^{bf}	<0.001
Tail moment (unit)	1.11±0.08	1.21±0.17	8.28±0.23 ^b	14.84±0.91 ^b	2.43±0.64 ^{ad}	9±0.39 ^{bf}	<0.001
Biochemical markers							
MDA#	0.60± 0.05	0.45± 0.06	2.71± 0.45 ^b	7.82± 0.68 ^b	1.47± 0.39 ^{ad}	3.91± 0.42 ^{bf}	<0.001
TAC#	8.71± 0.57	8.88± 0.53	2.87± 0.7 ^b	0.5± 0.17 ^b	7.57± 0.37 ^{ad}	2.93± 0.44 ^{bf}	<0.001

#: nmol/mg, One-way ANOVA, and Tukey HSD Post-hoc Test, P > 0.05: no significant differences, P < 0.05: significant differences, P < 0.001: highly significant differences.

a significant vs control group, b highly significant vs control group

c significant vs L(Pb) subgroup group, d highly significant vs L(Pb) subgroup group

e significant vs H(Pb) subgroup group, f highly significant vs H(Pb) subgroup group

TAC results analysis

TAC in the cerebellum was significantly lower in the L-Pb, H-Pb, L-Pb/Se, and H-Pb/Se subgroups than in the Se-free subgroup, according to biochemical analysis. Cerebellum TAC significantly increased when Pb and Se were combined in the L-Pb/Se and H-Pb/Se subgroups, respectively, compared to the L-Pb and H-Pb subgroups (Table 1).

H&E histopathological examination results

Examination of H&E-stained cerebellar sections of rats of Se-free and Se subgroups showed that the cerebellar cortex was formed of several folds or folia separated by narrow short and long sulci. The cerebellar cortex of each fold was conformed into three layers, arranged from superficial to deep; molecular cell layer, Purkinje cell layer and granular layer, beside less defined core of white matter (Fig. 1 A, C). The molecular cell layer showed normal eosinophilic (acidophilic) neuropil containing basket cells which located deep, and small stellate which located superficially. Purkinje cell layer displayed large pear-shaped (flask-shaped) and round-shaped cells with large rounded vesicular nuclei and prominent nucleoli and aligned in one row between the molecular cell

layer and the granular layer. Each Purkinje cell is surrounded by several Bergmann astrocytes. The granular layer contained a huge number of small deeply stained granular cells with acidophilic cerebellar islands or glomerulus (Fig.1 B, D).

Examination of H&E-stained cerebellar sections of rats of L-Pb subgroup showed the clearly defined three layers in cerebellar folia (Fig. 1E). The molecular layer showed blood vessels surrounded with wide perivascular spaces, stellate cells located superficially, and basket cells located deeply. The middle Purkinje layer showed large flask-shaped cells that were arranged in a single row with centrally located large nuclei, long axons and surrounded by Bergmann astrocytes. Few Purkinje neurons with darkly stained nuclei were also noticed. The inner granular layer showed small-packed rounded cell nuclei with acidophilic cerebellar islands (Fig. 2F).

H-Pb subgroup's H&E-stained cerebellar sections revealed severe disruption nearly in all layers. It revealed marked separated irregular pia matter and large dilated congested blood vessels (Fig. 1G). The molecular layer revealed blood vessels surrounded with wide perivascular spaces and their different neurons with darkly stained nuclei. The Purkinje layer revealed disturbed

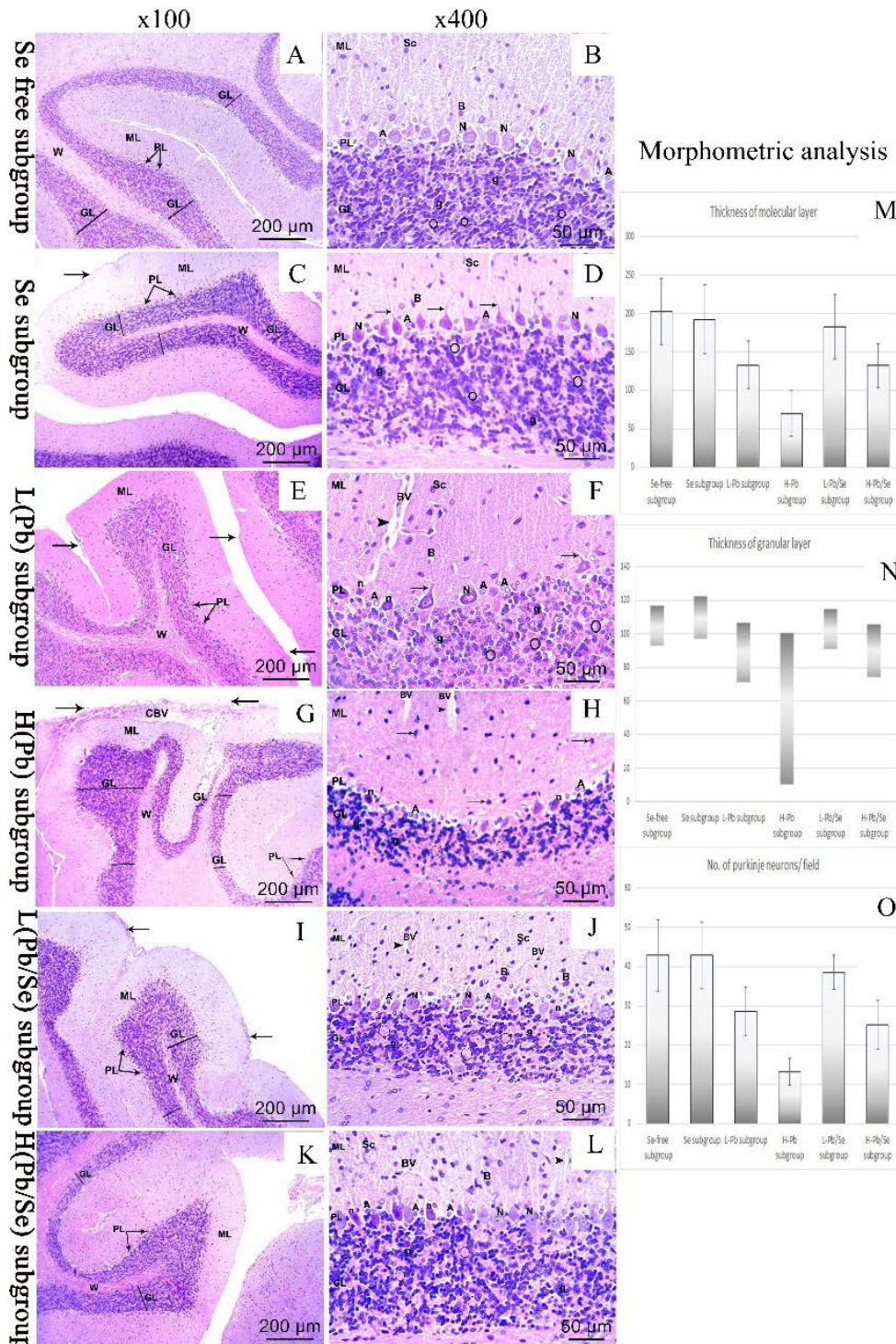


Fig. 1.- H&E Photomicrographs of the cerebellar tissue. (A,B Se-free subgroup; C,D Se subgroup; E,F L-Pb subgroup; G,H H-Pb subgroup; I,J L-Pb/Se subgroup; K,L H-Pb/Se subgroup (A, C, E, G, I, K) presenting the layers of the cerebellar cortex; the superficial molecular layer (ML), the deepest called granular (GL) and the Purkinje cells layer (PL) at the interface between the granular and molecular layers with inner white core of white matter (W). Pia matter (arrow) was irregular and separated in G and little separated in I, and large dilated congested blood vessels (CBV) in G. (B, D, F, H, J, L) presenting the outer molecular layer (ML) with deeply located basket cells (B) and superficially located small stellate (Sc). The middle Purkinje layer (PL) has large flask-shaped Purkinje cells that are arranged in a single row with centrally located large vesicular nuclei (N) and long axons (arrow) and surrounded by Bergmann astrocytes (A). The inner granular layer (GL) shows tightly or closely packed deeply stained rounded cell nuclei (g) with acidophilic cerebellar islands or glomerulus (circle), Bv; blood vessels, arrowheads; wide perivascular spaces, n; disturbed shrunken Purkinje cells with darkly stained nuclei and eosinophilic cytoplasm, rectangle; different neuron with darkly stained nuclei. (Scale bar: A, C, E, G, I, K: 200 µm, X 100; B, D, F, H, J, L: 50 µm, X 400. (M, O) charts show morphometrical assessment of molecular layer thickness and number of Purkinje cells. Data were expressed as mean ± SD. (N) chart shows morphometrical assessment of granular layer thickness. Data were expressed as as median (maximum-minimum).

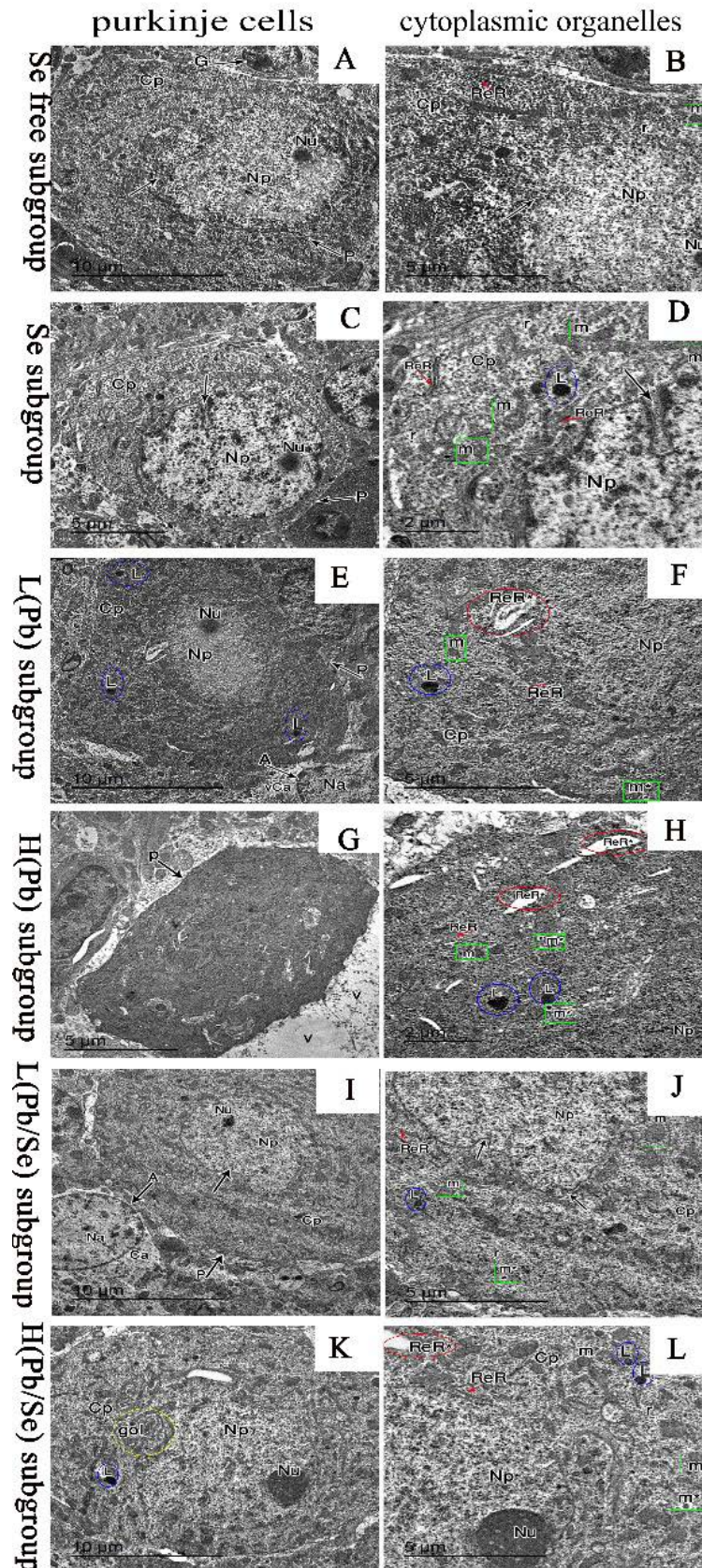


Fig. 2.- EM photomicrograph cerebellar tissue. (A,B Se-free subgroup; C,D Se subgroup; E,F L(Pb) subgroup; G,H H-Pb subgroup; I,J L-Pb/Se subgroup; K,L H-Pb/Se subgroup) (A, C, E, G, I, K) presenting purkinje cell (P) with euchromatic nucleus (Np) with indentation (arrow), prominent nucleolus (Nu), Golgi apparatus (gol). (B, D, F, H, J, L) presenting (Cp) containing rough endoplasmic reticulum (ReR), lysosomes (L), free ribosomes (r), marked dilated rough endoplasmic reticulum (ReR*), normal mitochondria (m) and small shrunken mitochondria with destructed cristae (m*), The surrounding neuropil showing vacuolations (V). (Scale bar: A: 10 μm, 800 X17; B, C: 5 μm, 1500 X17; D: 2 μm, 2000 X17).

shrunken Purkinje cells with darkly stained nuclei and eosinophilic cytoplasm and numerous Bergmann astrocytes. The granular layer showed scattered small, rounded cell nuclei with a wide expansion of acidophilic cerebellar islands (Fig. 1H).

H&E-stained cerebellar sections exhibited little separation in pia matter in L-Pb/Se subgroup. L-Pb/Se and H-Pb/Se subgroups' H&E-stained cerebellar sections revealed the clearly defined three layers (Fig. 1 I, K). The molecular and granular layers were normal. Purkinje layer showed a relatively normal linear appearance of Purkinje cells. Few Purkinje neurons were with undefined nuclei (Fig. 2 J, L).

Morphometric results

Regarding morphometric analysis for H&E-stained cerebellar sections, rats treated with Pb only (L-Pb and H-Pb) subgroups) showed significant decrease in molecular layer thickness, granular layer thickness and Purkinje neurons number/field. Combination of Pb with Se in L-Pb/Se subgroup showed a significant increase in molecular layer thickness, granular layer thickness and Purkinje neurons number/field in comparison with L-Pb subgroup, while there was no significant

difference with Se-free subgroup. Combination of Pb with Se in H-Pb/Se subgroup also showed a significant increase in molecular layer thickness, granular layer thickness and Purkinje neurons number/field in comparison with H-Pb subgroup, but there was significant decrease in molecular layer thickness, granular layer thickness and Purkinje neurons number/field in comparison with Se-free subgroup (-34.88%, -24.13%, -41.07% respectively) (Table 2, Fig. 1 M-O).

Ultrastructure examination of cerebellum

EM examination of cerebellar sections of rats of Se-free and Se subgroups revealed large flask shaped Purkinje cells with euchromatic nucleus with indentations and prominent nucleolus, cytoplasm had well developed strands of rough endoplasmic reticulum (RER), numerous mitochondria, and free ribosomes (Fig. 2 A-D). The granule cells had oval or rounded nuclei with coarse central and peripheral chromatin clumps, scanty cytoplasm containing mitochondria. The surrounding neuropil contained myelinated nerve fibers. The astrocyte cells with sharply demarcated nucleus and electron lucent cytoplasm containing mitochondria. The surrounding neuropil contained myelinated nerve fibers (Fig. 3 A-D).

Cerebellar sections of rats of L-Pb subgroup

Table 2. Morphometric analysis for H&E-stained cerebellar sections in different study groups.

	Control group		Pb group		Pb/Se group		P value
	Se-free subgroup	Se subgroup	L-Pb subgroup	H(Pb) subgroup	L-Pb/Se subgroup	H-Pb/Se subgroup	
Thickness of molecular layer^{*1}	202.68± 42.88	192.16±45.11	132.90± 30.63 ^a	70.10± 29.87 ^b	182.35± 42.12 ^c	131.99± 28.11 ^{ae}	<0.001
% of dif. #		-5.19%	-34.43%	-65.41%	-10.03%	-34.88%	
Thickness of granular layer^{*2}	107.55 (116.85-92.69)	104.82 (122.08-97.14)	93 (106.37-70.99) ^a	27.69 (100.54-10.22) ^b	101.53 (114.60-91.11) ^c	89.82 (105.76-74.37) ^{ae}	<0.001
% of dif. #		9.04%	-20.51%	-40.83%	-6.95%	-24.13%	
No. of Purkinje neurons/field^{*1}	42.85± 9.08	42.90± 8.44	28.60± 6.24 ^b	13.15± 3.40 ^b	38.50± 4.37 ^c	25.25± 6.19 ^{be}	<0.001
% of dif. #		0.12%	-33.26%	-69.31%	-10.15%	-41.07%	

*: at 100 magnifications, total 60 measurements for each subgroup were statistically assessed, &: at 400 magnification, total 30 measurements for each subgroup were statistically assessed, # % Of difference= mean of (each) group - mean of control group)/ mean of control group %

1 One-way ANOVA, and Tukey HSD Post-hoc Test to compare mean ± SD.

2 Kruskal Wallis H tests, and Mann-Whitney test to compare median.

P > 0.05: no significant differences, P < 0.05: significant differences, P < 0.001: highly significant differences.

a significant vs control group, b highly significant vs control group

c significant vs L(Pb) subgroup group, d highly significant vs L(Pb) subgroup group

e significant vs H(Pb) subgroup group, f highly significant vs H(Pb) subgroup group

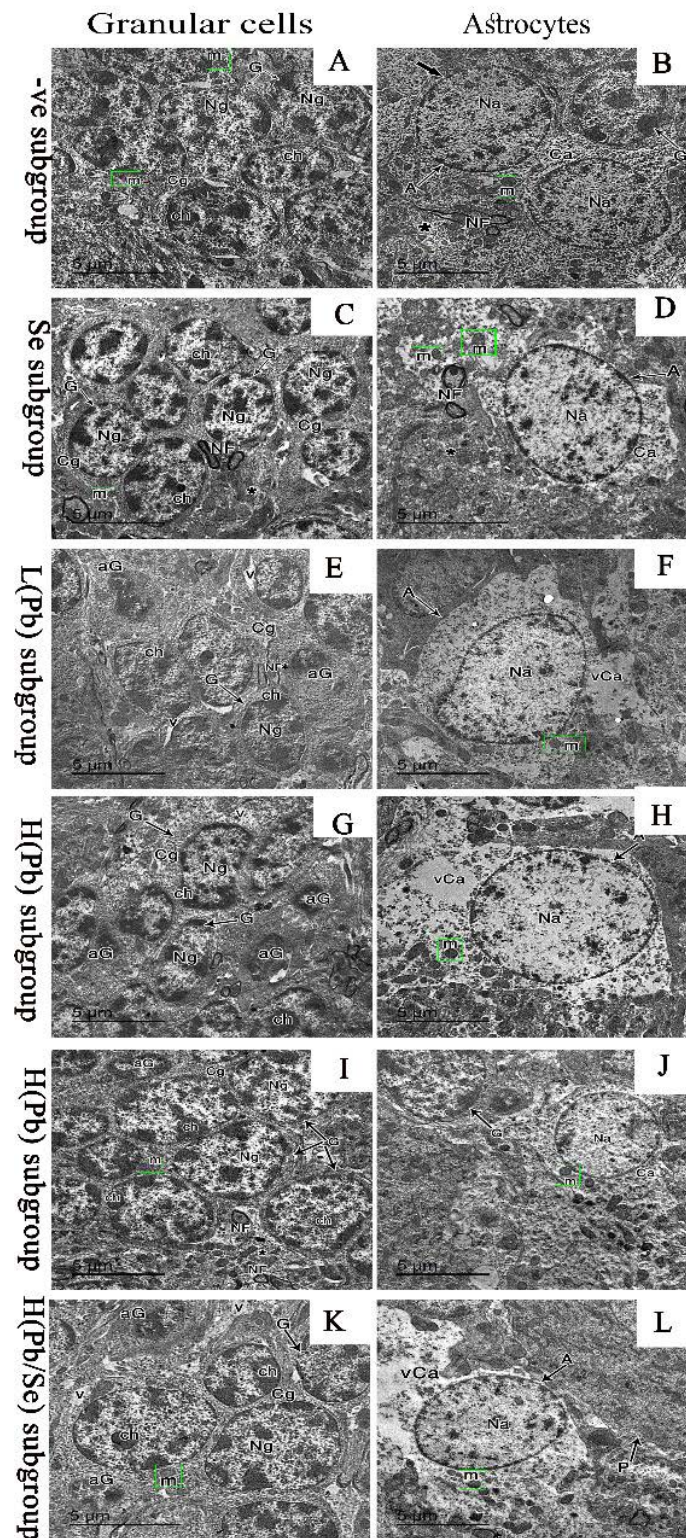


Fig. 3.- EM photomicrograph cerebellar tissue. (A, B Se-free subgroup; C, D Se subgroup; E, F L-Pb subgroup; G, H H(Pb) subgroup; I, J L-Pb/Se subgroup; K, L H-Pb/Se subgroup). (A, C) presenting granule cells (G) which have oval or rounded nuclei (Ng) with coarse central and peripheral chromatin clumps (ch) and scanty cytoplasm (Cg) containing mitochondria (m). The surrounding neuropil (*) contains myelinated nerve fibers (NF). (E, G, I, K) representing the granular layer containing some affected granule cells (aG) and normal granule cells (G) which have oval or rounded nuclei (Ng) with coarse central and peripheral chromatin clumps (ch) and vacuoles (V) in cytoplasm (Cg) containing mitochondria (m). The surrounding neuropil contains regularly myelinated nerve fibers (NF) and distorted myelinated nerve fibers (NF*). (B, D) electron micrographs representing astrocytes (A) with sharply demarcated (thick arrow) nucleus (Na) and electron lucent cytoplasm (Ca) containing mitochondria (m), the astrocyte presents near the granule cell (G). The surrounding neuropil (*) contains thick regularly myelinated nerve fibers (NF). (F, H, J, L) electron micrographs representing astrocytes (A) with sharp demarcated nucleus (Na) and electron lucent cytoplasm (Ca) containing mitochondria (m), vCa; vacuolated cytoplasm. (Scale bar: 5 µm, 1500 X17).

displayed Purkinje cells with hyperchromatic nucleus with prominent nucleolus; their cytoplasm contained mild dilated RER, small dense mitochondria with destructed cristae and multiple lysosomes (Fig. 2 E, F). Some granular cells were normal and affected granule cells that were small, irregular, and showed increased condensation of nuclear chromatin. The surrounding neuropil was containing distorted myelinated nerve fibers. The astrocyte cells showed vacuolated cytoplasm containing mitochondria (Fig. 3 E, F). In H-Pb subgroup, Purkinje cells lost their normal structure displayed ill-defined nucleus with dark cytoplasm (Fig. 2 G, H). Many affected granule cells were small, irregular, and showed increased condensation of nuclear chromatin. The surrounding neuropil contained distorted myelinated nerve fibers and showed separation in myelin sheath. The astrocyte cells showed vacuolated cytoplasm containing mitochondria (Fig. 3 G, H).

L-Pb/Se subgroup's cerebellar sections showed Purkinje cells that had euchromatic nucleus, and their cytoplasm contained strands of RER, small

dense mitochondria with destructed cristae and free ribosomes (Fig. 2 I, J). Many normal granular cells and little affected granule cells were detected. The astrocytes were normal (Fig. 3 I, J). Moreover, H-Pb/Se subgroup's cerebellar sections displayed Purkinje cells that had euchromatic nucleus with prominent nucleolus, their cytoplasm containing well-developed and mildly dilated strands of RER, well-developed and small dense mitochondria with destructed cristae, well-developed Golgi apparatus, numerous lysosomes, and free ribosomes (Fig. 2 K, L). The granular cells contained rounded or oval nuclei with central and peripheral clumped chromatin; their cytoplasm was vacuolated and affected granule cells. The astrocyte cytoplasm was vacuolated (Fig. 3 K, L).

GFAP Immunoreactivity results

Examination of GFAP-stained cerebellar sections of rats of Se-free and Se subgroups showed a positive GFAP-staining in the cytoplasm and processes of astrocytes; they appear small with thin, few short processes. In the molecular layer, a

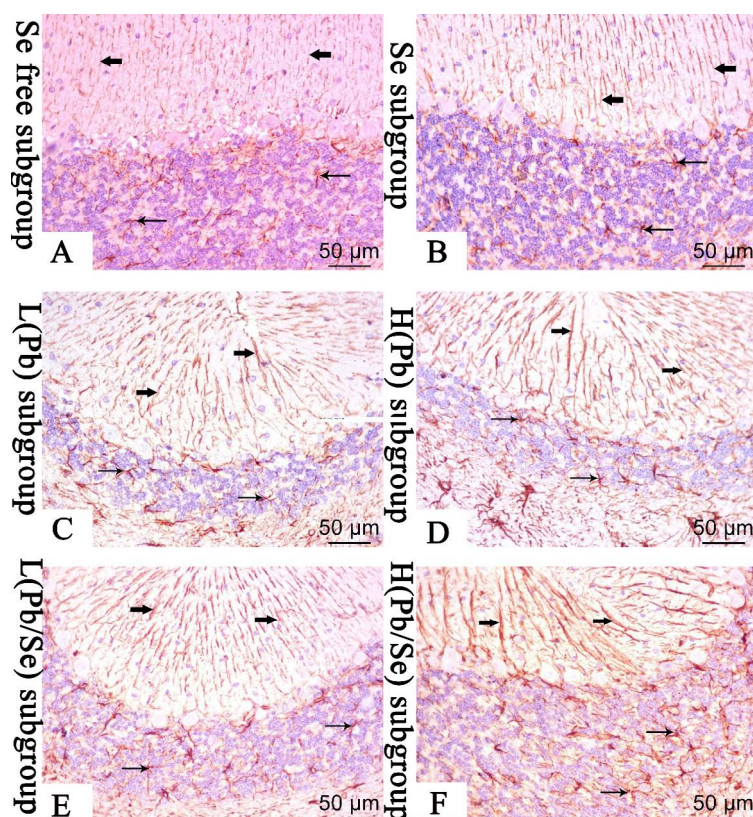


Fig. 4.- Immunohistochemical staining for anti-GFAP; (A Se-free subgroup; B Se subgroup; C L(Pb) subgroup; D H-Pb subgroup; E L-Pb/Se subgroup; F H-Pb/Se subgroup) stained cerebral sections showing a positive GFAP-staining in the cytoplasm and processes of astrocytes (arrow) which appear small with thin, few short processes in (A,B,E) variable size with thick, long, branched processes in (C), multiple, thick, long, branched processes in (D), appear with multiple, thick branched processes in (F). In molecular layer, a positive staining in processes of Bergman cells (thick arrow) which appear few, long thin processes in (A,B), numerous, thick long processes in (D,F) numerous with variable size process in (C,E). (Scale bar: A-F: 50 μ m, X400).

positive GFAP-staining in processes of Bergmann cells appeared few, long, and thin. Examination of GFAP-stained cerebellar sections of rats of L(Pb) subgroup showed a positive GFAP-staining in the cytoplasm and processes of astrocytes; they appear numerous, with multiple, thick processes. In the molecular layer, a positive staining in Bergmann cells' processes appeared numerous, long, and thin. In L(Pb/Se) subgroup, the cytoplasm and processes of astrocytes, they appear numerous with multiple, thin processes. In the molecular layer, a positive staining in the processes of Bergmann cells appeared numerous, long and thin. Moreover, in H(Pb) and H(Pb/Se) subgroups, there was abundant positive GFAP-staining in the cytoplasm and processes of astrocytes; they appear numerous, with multiple, thick processes. In the molecular layer, a positive staining in processes of Bergmann cells appeared numerous, thick, and long (Fig. 4 A-F).

DISCUSSION

Pb is a hazardous heavy metal that is ubiquitous in the human environment, and poses significant health risks, especially to children, due to its multiple and distinct physical and chemical properties (Harshitha et al., 2024). The brain is sensitive to the oxidative stress of Pb, because it consumes a high percentage of oxygen (Ren et al., 2022). Our research investigated the neurotoxic effects on the cerebellum of rats, resulting from daily oral Pb consumption at low and high levels. To this end, we selected male rats to avoid any potential effects of estrous hormonal changes that may occur in adult female animals on the study results (Hegazy et al., 2020).

Through our biochemical results, the level of oxidative stress was assessed through TAC, as well as MDA, which is the end product of polyunsaturated fatty acid oxidation (Cordiano et al., 2023). The biochemical results obtained showed a significant decline in TAC and a significant increase in MDA level in the cerebellum of rats treated with Pb only (L-Pb and H-Pb subgroups) compared to control groups. These outcomes are in synchronization with results of other authors (Udi et al., 2022). The high level of MDA can be attributed to the generation of a highly reactive hydroxyl

radical (OH), which extracts hydrogen ions from fatty acids, leading to the formation of fatty acid radicals. The accumulation of these free radicals weakens the integrity of the membrane, ultimately leading to cell damage. These findings impacted the histological findings in the Pb-consuming subgroups. There was marked, separated, irregular pia matter and large dilated, congested blood vessels in H&E examination that were more evident in H-Pb subgroup. This separation may be due to a change in permeability and a disturbance in blood dynamics, leading to leakage of fluid into the cerebellar tissue due to oxidative stress. Oxidative stress also impacted on GFAP immunoreactivity. Astrocytes are the direct target of Pb toxicity (Cai et al., 2019). GFAP is an intermediate filament protein expressed by various cell types of the central nervous system (CNS), including astrocytes (El-Beltagy et al., 2022). Increased levels of GFAP in astrocytes were thought to be a feature of astrocytes reacting to oxidative damage (reactive gliosis), which has been described in many neurodegenerative conditions (Bekheet, 2020). The results of the present work showed a significant positive immunohistochemical staining for GFAP in the cytoplasm and processes of astrocytes, which appeared numerous with multiple and thick processes. There was also positive staining in the processes of the Bergmann cells of the molecular layer, which appeared numerous, thick, and elongated, all findings were more pronounced in the H-Pb subgroups than in the L-Pb subgroups.

Biochemically, our experiment recorded a significant increase in DNA fragmentation, leading to increased incidence of apoptosis, a result consistent with Nam et al. (2018), who noted that Pb intake can increase the apoptosis factor Bcl-2-associated X protein (BAX) and DNA fragmentation in the cerebellum. These findings regarding apoptosis were confirmed in H&E-stained cerebellar sections in the present study. Examination of the different neurons showed darkly stained nuclei, and the Purkinje layer revealed shrunken, disordered Purkinje cells with darkly stained nuclei and eosinophilic cytoplasm and numerous Bergmann astrocytes. Further morphometric analysis for H&E-stained cerebellar sections showed that rats

treated with Pb only (L-Pb and H-Pb subgroups) had a significant decrease in the thickness of both the molecular and granular layers, as well as a significant decrease in number of Purkinje neurons, which also approved Pb apoptotic effect.

Ultrastructural examination also revealed several morphological changes where the neuropil contained distorted myelinated nerve fibers, and showed detachment of the myelin sheath. According to Duncan et al. (2021), the production and maintenance of myelin is critical to normal CNS function. Small changes in myelin could lead to changes in conduction speed, which is serious for the correct function of integrated neuronal circuits. EM examination of cerebellar sections from Pb-treated rats (L-Pb and H-Pb subgroups) confirmed the histological findings of H&E-stained sections. Purkinje cells had an irregular, hyperchromatic nucleus with prominent nucleoli; the dark cytoplasm contained marked dilated RER, numerous lysosomes, and small, dense mitochondria with destructed cristae. The affected granule cells were small, irregular, and showed increased condensation of nuclear chromatin and vacuoles in cytoplasm. The astrocyte cells contained sharp demarcated nucleus with chromatin and vacuolated cytoplasm containing mitochondria.

In an attempt to protect the cerebellar cortex from the neurotoxic effects of Pb, we investigated the potential mitigating effects of Se that have been previously investigated in the cerebrum (Hegazy et al., 2023). Biochemical statistics strengthened the powerful antioxidant activity of Se, as there was a significant decline in MDA level, with a significant increase in TAC level in cerebellar tissue of rats treated with Pb and Se (L-Pb/Se and H-Pb/Se subgroups), in contrast with subgroups treated with Pb only with more protection in L-Pb/Se subgroup. The Se antioxidant effect was also demonstrated in GFAP-stained sections of Pb and Se-treated groups. GFAP positive staining was found in the cytoplasm and processes of astrocytes; they appear numerous with multiple, thick processes. In the molecular layer, there was a positive staining in Bergmann cell processes that appeared numerous, long and thin, and this result is consistent with Bekheet (2022), who reported the protective role of Se against long-term phenytoin

administration.

Moreover, the co-administration of Se with Pb improved the histopathological changes of H&E-stained sections of cerebellar cortex and protected the cerebellum from the Pb-apoptotic effect. This was signified by clearly defined three layers in the folia, with the inner white core of the white matter. The molecular layer appeared normal, with blood vessels that had narrow perivascular spaces. The Purkinje layer showed a relatively normal linear appearance of Purkinje cells; most of these cells preserved their normal flask shape, with centrally located large nuclei and basophilic cytoplasm, and surrounded by Bergmann astrocytes. This was confirmed by increased thickness of molecular and granular layer thickness and number of Purkinje neurons morphometrically. EM examination of Pb/Se group (L-Pb/Se and H-Pb/Se subgroups) also showed improvement in Purkinje cells. Purkinje cells had an euchromatic nucleus, with indentations and prominent nucleolus, their cytoplasm containing strands of rough endoplasmic reticulum, small dense mitochondria with destructed cristae and free ribosomes. Most granular cells had a normal appearance. The protective effect of Se was also proved by a significant decrease in DNA fragmentation percentage in Pb/Se group (L-Pb/Se and H-Pb/Se subgroups). Consistent with our results, Se anti-apoptotic effect in other tissues has also been reported by Mehanna et al. (2022), who proved that administration of Se nanoparticles downregulated the expression of the proapoptotic agents BAX, caspase 3 and caspase 9 in the rat kidney after vancomycin treatment.

Referring to the previous study on the cerebral cortex (Hegazy et al., 2023), the effects of Pb exposure and Se protection differ in the cerebral and cerebellar cortices. Pb exposure (at both low and high doses) significantly causes DNA fragmentation, lipid peroxidation, and decreased TAC in both cortices, leading to disruption of tissue structures. In the cerebral cortex, Pb causes neuronal shrinkage with vacuole formation and glial cell reactivity, while in the cerebellar cortex, Pb leads to Purkinje cell degeneration and impaired granule layers. Se co-administration mitigates these effects by reducing oxidative damage, re-

storing TAC, and improving structural integrity. However, the extent of recovery varies, with the cerebellar cortex showing better histological and morphometric restoration compared to the cerebral cortex. The cerebellar cortex's better recovery reflects a region-specific response to Se, which may be influenced by its simpler organization, different metabolic demands, and unique antioxidant profiles.

Protective effect of Se in our study was more effective in L-Pb/Se subgroup at a dose of 0.25 mg/kg/day daily for 4 weeks which contrasted with Rahbardar et al. (2021), who reported protective effect of Se at a dose of 0.6 mg/kg/day. Our used dose of Se is more accessible as daily supplementation according to Majeed et al. (2022), who reported that Se deficiency is reported to affect 500 million to one billion people worldwide, mainly due to inadequate dietary intake of Se.

In conclusion, Pb-induced neurotoxicity is significantly influenced by the pathways of oxidative stress and apoptosis. Se controls oxidative stress and apoptosis, hence protecting the cerebellum from Pb-induced histopathological alterations. It has been proposed that Se can assist overcome Pb-induced neurotoxicity.

ABBREVIATIONS

BAX	Bcl-2-associated X protein
BBB	Blood-brain barrier
CNS	Central nervous system
EM	Electron microscopy
GFAP	Glial fibrillary acidic protein
H&E	Hematoxylin and Eosin
H-Pb	High dose lead subgroup
H-Pb/Se	High doses lead and selenium subgroup
LM	Light microscopy
L-Pb	Low doses lead subgroup
L-Pb/Se	Low doses lead and selenium subgroup
MDA	Malondialdehyde
OH	Reactive hydroxyl radical
Pb	Lead
PBS	Phosphate buffered saline
RER	Rough endoplasmic reticulum
Se	Selenium
TAC	Total antioxidant capacity

Ethics approval and consent to participate

All studies and procedures involving rats were approved by Institutional Animal Care and Use Committee at Zagazig University in Egypt (ZU-IA-CUC/3/F/93/2020) and by the National Institute of Health (NIH) guidelines. Consent for publication: the publication of this manuscript has been approved by all authors.

ACKNOWLEDGEMENTS

We would like to thank Dr. Hosnia M. Ragab, Professor of Public Health and Community Medicine at the Faculty of Medicine, Zagazig University, for her assistance in conducting the statistical analysis. We would like to extend our special thanks to the members of the Institutional Animal Care and Use Committee (IACUC) at Zagazig University and the Vice Dean of Scientific Research at the Faculty of Medicine, Zagazig University, Egypt. Artificial intelligence (AI) is not used in this paper in any way.

REFERENCES

- ADEDARA IA, FABUNMI AT, AYENITAJU FC, ATANDA OE, ADEBOWALE AA, AJAYI BO, OWOEYE O, ROCHA JBT, FAROMBIEO (2020) Neuroprotective mechanisms of selenium against arsenic-induced behavioral impairments in rats. *Neurotoxicology*, 76: 99-110.
- ADEMUYIWA O, UGBAJA RN, ROTIMI SO, ABAM E, OKEDIRAN BS, DOSUMU OA, ONUNKWOR BO (2007) Erythrocyte acetylcholinesterase activity as a surrogate indicator of lead-induced neurotoxicity in occupational lead exposure in Abeokuta, Nigeria. *Environ Toxicol Pharmacol*, 24(2): 183-188.
- ALI HFH, EL-SAYED NM, KHODEER DM, AHMED AAM, HANNA PA, MOUSTAFA YMA (2020) Nano selenium ameliorates oxidative stress and inflammatory response associated with cypermethrin-induced neurotoxicity in rats. *Ecotoxicol Environ Saf*, 195: 110479.
- BANCROFT JD, GAMBLE A (2008) *Theory and practice of histological techniques*. 6th edition. Churchill Livingstone/ Elsevier Health Sciences, pp 165-175.
- BATY RS, HASSAN KE, ALSHARIF KF, EL-HENNAMY RE, ELMAHALLAWY EK, HAFEZ MM, MONEIM AA, KASSAB RB (2020) Neuroprotective role of luteolin against lead acetate-induced cortical damage in rats. *Hum Exp Toxicol*, 39(9): 1200-1212.
- BEKHEET EA (2020) The possible protective role of selenium against long-term phenytoin administration effects on cerebellar cortex of adult male albino rats: Histological and immunohistochemical study. *Egypt J Histol*, 43(2): 509-518.
- CAI S, LIU J, SHI X, HU S, ZHAO L (2019) Allicin alleviated learning and memory deficits caused by lead exposure at developmental stage. *Life Sci*, 231: 116532.
- CAREY MR (2024) The cerebellum. *Curr Biol*, 34(1): 7-11.
- CHOI J, KIM YS, KIM MH, KIM HJ, YOON BE (2022) Maternal lead exposure induces sex-dependent cerebellar glial alterations and repetitive behaviors. *Front Cell Neurosci*, 16: 954807.
- CORDIANO R, DI GIOACCHINO M, MANGIFESTA R, PANZERA C, GANGEMI S, MINCIULLO PL (2023) Malondialdehyde as a potential oxidative stress marker for allergy-oriented diseases: an update. *Molecules*, 28(16): 5979.
- DUNCAN GJ, SIMKINS TJ, EMERY B (2021) Neuron-oligodendrocyte interactions in the structure and integrity of axons. *Front Cell Dev Biol*, 9: 653101.

- EL-BELTAGY AEFB, ABDELAZIZ KK, SALEH AM, ELSAYYAD HI, GAHNEM RA (2022) Evaluation of lead toxicity on the retina of pregnant rats and their pups: the possible ameliorative role of pomegranate juice. *F1000Research* 11(461).
- GALAL MK, ELLEITHY EMM, ABDRABOU MI, YASIN NAE, SHAHEEN YM (2019) Modulation of caspase-3 gene expression and protective effects of garlic and spirulina against CNS neurotoxicity induced by lead exposure in male rats. *Neurotoxicology*, 72: 15-28.]
- GENCHI G, LAURIA G, CATALANO A, SINICROPI MS, CAROCCI A (2023) Biological activity of selenium and its impact on human health. *Int J Mol Sci*, 24(3): 2633.
- GHADERI S, KOMAKI A, SALEHI I, BASIR Z, RASHNO M (2023) Possible mechanisms involved in the protective effects of chrysin against lead-induced cognitive decline: An in vivo study in a rat model. *Biomed Pharmacother*, 157: 114010.]
- HAMDAN M, NOORHAMDANI AS, RAHAYU M, MACHFOED MH (2020) The effect of ginkgo biloba (Eg) extracts on the expression of Hsp 90, Vegf and Bdnf in the Rattus Novergicus with lead (Pb) exposure. *J Int Dent Med Res*, 13(1): 17-22.
- HARSHITHA P, BOSE K, DSOUZA HS (2024) Influence of lead-induced toxicity on the inflammatory cytokines. *Toxicology*, 503: 153771.
- HEGAZY AA, DOMOUKY AM, AKMAL F, EL-WAFAEY DI (2023) Possible role of selenium in ameliorating lead-induced neurotoxicity in the cerebrum of adult male rats: an experimental study. *Sci Rep*, 13(1): 15715.
- HEGAZY R, HEGAZY A (2015) Hegazy's simplified method of tissue processing (consuming less time and chemicals). *Ann Int Med Dent Res*, 1(2): 57-61.
- HEGAZY AA, ABD AL HAMEED EA, EL-WAFAEY DI, KHORSHEED OA (2020) Potential role of Moringa Oleifera in alleviating paracetamol-induced nephrotoxicity in rat. *Eur J Anat*, 24(3): 179-191.
- IACUC (2014) Institutional Animal Care and Use Committee. Available at: <https://research.iu.edu/doc/compliance/animal-care/iupui/iupui-iacuc-use-of-non-pharmaceutical-grade-chemicals-compounds.pdf>
- KHALIL HS, MAULU S, VERDEGEM M, ABDEL-TAWWAB M (2023) Embracing nanotechnology for selenium application in aquafeeds. *Rev Aquac*, 15(1): 112-129.
- LI S, YANG C, YI X, WEI R, ASCHNER M, JIANG Y, OU S, YAO C (2023) Effects of sub-chronic lead exposure on essential element levels in mice. *Biol Trace Elem Res*, 201: 282-293.
- MA YM, IBEANU G, WANG LY, ZHANG JZ, CHANG Y, DONG JD, JING L (2017) Selenium suppresses glutamate-induced cell death and prevents mitochondrial morphological dynamic alterations in hippocampal HT22 neuronal cells. *BMC Neurosci*, 18(1): 15.
- MAJEED M, NAGABHUSHANAM K, PRAKASAN P, MUNDKUR L (2022) Can selenium reduce the susceptibility and severity of SARS-CoV-2? A comprehensive review. *Int J Mol Sci*, 23(9):4809.
- MEHANNA ET, KHALAF SS, MESBAH NM, ABO-ELMATTY DM, HAFEZ MM (2022) Anti-oxidant, anti-apoptotic, and mitochondrial regulatory effects of selenium nanoparticles against vancomycin induced nephrotoxicity in experimental rats. *Life Sci*, 288: 120098.
- NAM SM, CHANG BJ, KIM JH, NAHM SS, LEE JH (2018) Ascorbic acid ameliorates lead-induced apoptosis in the cerebellar cortex of developing rats. *Brain Res*, 1686: 10-18.
- NEHRU B, KANWAR SS (2004) N-acetylcysteine exposure on lead-induced lipid peroxidative damage and oxidative defense system in brain regions of rats. *Biol Trace Elem Res*, 101(3): 257-264.
- NILI-AHMADABADI A, ALI-HEIDAR F, RANJBAR A, MOUSAVI L, AHMADIMOGHADDAM D, LARKI-HARCHEGANI A, GHAFOURI-KHOSROSHAHI A (2018) Protective effect of amlodipine on diazinon-induced changes on oxidative/antioxidant balance in rat hippocampus. *Res Pharm Sci*, 13(4): 368.
- OLGAG, IRITR, JOSEPH W, OFER B (2002) Role of myocardial inducible nitric oxide synthase in contractile dysfunction and β -Adrenergic hyporesponsiveness in rats with experimental volume –overload heart failure circulation. *J Am Heart Assoc*, 105(2): 236-243.
- PHARES TW, KEAN RB, MIKHEEVA T, HOOPER DC (2006) Regional differences in blood-brain barrier permeability changes and inflammation in the apathogenic clearance of virus from the central nervous system. *J Immunol*, 176(12):7666-7675.
- PRATI JM, PONTES-SILVA A, GIANLORENÇO ACL (2024) The cerebellum and its connections to other brain structures involved in motor and non-motor functions: A comprehensive review. *Behav Brain Res*, 465: 114933.
- RAHBARDAR M, FARMAD C, HOSSEINZADEH H, MEHRI S (2021) Protective effects of selenium on acrylamide-induced neurotoxicity and hepatotoxicity in rats. *Iran J Basic Med Sci*, 24(8): 1041-1049.
- RALSTON NV, RAYMOND LJ (2010) Dietary selenium's protective effects against methylmercury toxicity. *Toxicol*, 278(1): 112-123.]
- RANJBAR Z, POURHADADI D, MONTAZERI SH, ROSHANZAMIR MM (2023) Lead compounds in paint and coatings: A review of regulations and latest updates. *Prog Org Coat*, 174: 10724.
- REN Y, SUN-WATERHOUSE D, OUYANG F, TAN X, LI D, XU L, LI B, WANG Y, LI F (2022) Apple phenolic extracts ameliorate lead-induced cognitive impairment and depression-and anxiety-like behavior in mice by abating oxidative stress, inflammation and apoptosis via the miR-22-3p/SIRT1 axis. *Food Funct*, 13(5): 2647-2661.
- SALMAN SA, ASMOAY AA, EL-GOHARY A, SABETH H (2019) Evaluation of human risks of surface water and groundwater contaminated with Cd and Pb in the southern El-Minya Governorate, *Egypt. Drink Water Eng Sci*, 12: 23-30.
- SINGH PK, SINGH MK, YADAV RS, NATH R, MEHROTRA A, RAWAT A, DIXIT RK (2017) Omega-3 fatty acid attenuates oxidative stress in cerebral cortex, cerebellum, and hippocampus tissue and improves neurobehavioral activity in chronic lead-induced neurotoxicity. *Nutr Neurosci*, 22(2): 83-97.
- TICE RR, AGURELL E, ANDERSON D, BURLINSON B, HARTMANN A, KOBAYASHI H, MIYAMAE Y, ROJAS E, RYU JC, SASAKI YF (2000) Single cell gel/comet assay: guidelines for in vitro and in vivo genetic toxicology testing. *Environ Mol Mutagen*, 35(3): 206-221.
- UDI OA, OYEM JC, EBEYE OA, CHRIS-OZOKO LE, IGBIGBI PS, OLANNYE DU (2022) The effects of aqueous extract of ocimum gratissimum on the cerebellum of male Wistar rats challenged by lead acetate. *Clin Nutr Open Sci*, 44: 28-41.]
- ULLAH H, LIU G, YOUSAF B, ALI MU, ABBAS Q, MUNIR MAM, MIAN MM (2018) Developmental selenium exposure and health risk in daily foodstuffs: a systematic review and meta-analysis. *Ecotoxicol Environ Saf*, 149: 291-306.
- WANG F, LIU Z, XIE R, JU X, WANG W, PAN D, CHU L (2023) Poly (N-isopropylmethacrylamide-co-4-acrylamidobenzo-18-crown-6) microgels with expanded networks for excellent adsorption of lead (II) ions. *Particuology*, 77: 105-115.
- XU J, LI Y, WANG S, LONG S, WU Y, CHEN Z (2023) Sources, transfers and the fate of heavy metals in soil-wheat systems: The case of lead (Pb)/zinc (Zn) smelting region. *J Hazard Mater*, 5(441): 129863.
- ZHUO Z, WANG H, ZHANG S, BARTLETT PF, WALKER TL, HOU ST (2023) Selenium supplementation provides potent neuroprotection following cerebral ischemia in mice. *J Cereb Blood Flow Metab*, 43(7): 1060-1076.]